



# Dependence of photoluminescence on sulfurization temperature of $\text{Cu}_2\text{SnS}_3$ thin films

Kunihiko Tanaka<sup>1</sup> · Shogo Miyagi<sup>1</sup> · Daiki Motai<sup>2</sup> · Ryota Ohashi<sup>2</sup> · Yoko Hosokawa<sup>2</sup> · Kazuo Jimbo<sup>2</sup> · Yoji Akaki<sup>3</sup> · Hideaki Araki<sup>2</sup>

Received: 24 October 2022 / Accepted: 10 April 2023 / Published online: 18 April 2023  
© The Author(s), under exclusive licence to Springer-Verlag GmbH, DE part of Springer Nature 2023

## Abstract

The dependence of photoluminescence (PL) on sulfurization temperature of the  $\text{Cu}_2\text{SnS}_3$  (CTS) thin films was investigated. CTS thin films were prepared at various sulfurization temperatures in the range of 500–600 °C, and differences in the conversion efficiency of solar cells with the CTS thin films as absorption layer and the crystal structure of the CTS thin films were observed. In low-conversion-efficiency CTS films, which were a mix of monoclinic and cubic crystals, the PL spectrum only showed donor–acceptor pair (DAP) recombination luminescence due to deep defects. In high-conversion-efficiency CTS thin films, which contained only monoclinic crystals, the PL spectrum showed DAP recombination luminescence originating from the same deep defects. In addition band-edge luminescence was observed at room temperature. Thus, it was found that the conversion efficiency and crystal structure of CTS thin film can be easily estimated from PL measurements.

**Keywords**  $\text{Cu}_2\text{SnS}_3$  · Photoluminescence · Thin film solar cell · Exciton luminescence · Donor–acceptor pair (DAP) recombination luminescence · Crystal structure

## 1 Introduction

The p-type semiconductors  $\text{CuIn}_{1-x}\text{Ga}_x\text{Se}_2$  (CIGS) and CdTe have been widely studied as absorption layers in thin-film solar cells. However, these materials have environmental and safety issues, because they contain elements of low abundance (In, Ga, Te) and toxic (Se, Cd) elements.

$\text{Cu}_2\text{SnS}_3$  (CTS) is attracting attention as a material to solve these problems. CTS is composed of abundant and harmless elements and has a large absorption coefficient of  $10^4 \text{ cm}^{-1}$  or more. Kuku and Fakolujo [1] were the first to report thin-film solar cells using CTS; their Schottky solar

cells had a conversion efficiency of 0.11%. There have been many reports on CTS-based thin-film solar cells having conversion efficiencies higher than 4% [2–6]. The maximum conversion efficiency of current CTS solar cells is 5.24%, achieved by Kanai et al. [7]. This is far below the theoretical limit of CTS, which is about 25% [8].

One of reasons for the low efficiency compared with the theoretical limit is that CTS has several crystal structures. Generally, the crystal structure of CTS depends on the growth temperature, where cubic CTS is formed at high temperature ( $> 775 \text{ °C}$ ), and monoclinic, triclinic, and tetragonal crystals are formed at lower temperatures ( $< 775 \text{ °C}$ ) [9–11]. This fact means that the growth temperature is a very important factor determining the crystal structure. The band gap energy  $E_g$  of CTS is about 0.9–1.6 eV [12–15], depending on the crystal structure. Fernandes et al. [13] changed the maximum temperature of sulfurization and investigated the phase changes in CTS. As a result,  $E_g$  was found to be 1.35 eV and 0.96 eV for tetragonal and cubic crystals at sulfurization temperatures of 350 and 400 °C, respectively. The structure of CTS used in thin-film solar cells is generally monoclinic [2, 4, 5, 16], and there is no report on high-efficiency CTS solar cells with CTS phases other than monoclinic.

✉ Kunihiko Tanaka  
tanaka@vos.nagaokaut.ac.jp

<sup>1</sup> Department of Electrical, Electronics and Information Engineering, Nagaoka University of Technology, 1603-1, Kamitomioka, Nagaoka, Niigata 940-2188, Japan

<sup>2</sup> National Institute of Technology (KOSEN), Nagaoka College, 888 Nishikataka, Nagaoka, Niigata 940-8532, Japan

<sup>3</sup> National Institute of Technology (KOSEN), Miyakonojo College, 473-1 Yoshio, Miyakonojo, Miyazaki 885-8567, Japan

Addition of Na is also effective in increasing the conversion efficiency. Nakashima et al. [5] prepared Na-modified CTS thin films by changing the NaF molar ratio in NaF/Cu/Sn layered precursors and investigated the effect of Na addition on CTS solar cells. As a result, the fill factor, short-circuit current density, open-circuit voltage, and conversion efficiency were found to increase as the NaF/Cu molar ratio in the precursor increased. Among these samples, the highest conversion efficiency of 4.63% was obtained when the NaF/Cu ratio was 0.075. In ref. [7], which reported the highest conversion efficiency in CTS-based solar cells, Na was also added to improve conversion efficiency. Thus, the addition of Na greatly contributes to improving the performance of CTS solar cells. According to refs [16, 17], increasing the conversion efficiency of CTS solar cells requires a Cu-poor (Cu/Sn < 2.0) composition. Therefore, the key to improving the conversion efficiency of CTS-based solar cells is a Cu-poor composition (Cu defects), monoclinic crystal structure and Na addition.

Since photoluminescence (PL) is very sensitive to defects and PL contains information on defect levels, observation of PL is an important analysis method to investigate defect levels in semiconductors. Therefore, PL observation of Na-modified and Cu-poor CTS is very important. In addition, since the band gap energy of CTS depends on the crystal structure, the PL of CTS is affected by the crystal structure; therefore, the observation of PL as a function of crystal structure is important.

In our previous work, PL spectroscopy was used to evaluate CTS. In Ref. [18], the defect levels in Cu-poor (Cu/Sn = 1.8) monoclinic CTS thin films were investigated by measuring PL. CTS thin films were prepared by co-evaporation of Cu, Sn and S. The PL showed peaks at 0.843 and 0.867 eV and the peaks were attributed to donor–acceptor pair (DAP) recombination luminescence; the thermal activation energies associated with the peaks were 22.9 and 24.8 meV, respectively.

In ref [19], bulk single crystals of single-phase monoclinic CTS were prepared by the iodine transport method with a quenching process. The observed PL from the monoclinic CTS single crystals showed free exciton luminescence at 0.9317 eV and two bound exciton luminescence peaks at 0.9291 and 0.9260 eV at 4.2 K. The activation energy of the free exciton was 6.5 meV, and from the activation energy and free exciton luminescence energy, the band gap energy of monoclinic CTS was determined to be 0.94 eV [20].

In ref [21], poly-crystalline samples of Cu-poor, stoichiometric, and Cu-rich CTS with or without Na addition were prepared by solid-state reaction, and the PL spectra of the CTS samples were measured. Exciton luminescence was observed from only the Cu-rich samples, while DAP luminescence was observed from all samples. The estimated activation energy of the DAP was smaller with Na than without

Na. Therefore, it was concluded that Na addition increased the carrier density due to the acceptor level approaching the valence band.

As mentioned above, we investigated the PL of CTS thin films and bulk poly- and single-crystalline samples. However, differences in PL caused by differences in conversion efficiency and crystal structure had not been investigated. In this work, Cu-poor and Na-modified CTS thin films containing only monoclinic CTS or both monoclinic and cubic CTS were prepared by changing the sulfurization temperature; also, using the CTS thin films, CTS solar cells with different conversion efficiencies were prepared. Then, differences in PL caused by differences in conversion efficiency and crystal structure were investigated.

## 2 Experimental method

The samples used in this study were prepared as follows. A Mo layer with a thickness of approximately 0.8  $\mu\text{m}$  was DC sputtered onto an alkali-free glass substrate as the bottom electrode. Sn (340 nm, 99.9999%) and Cu (260 nm, 99.9999%) were deposited on alkali-free glass/Mo by electron beam evaporation at a substrate temperature of 130  $^{\circ}\text{C}$  and in a vacuum of  $7.5 \times 10^{-4}$  Pa or less. On this Sn/Cu stacked precursor, 10 mg of NaF (NaF, 99%) was vacuum deposited using a vacuum deposition apparatus (ULVAC KIKO, Inc., VPC-260F) equipped with a Mo resistance heating boat (Nilaco Corp., T-202M). The distance between the deposition source (NaF) and the sample stacked precursor was about 190 mm. The alkali-free glass /Mo/Sn/Cu/NaF precursor was placed in a quartz container with 100 mg of sulfur (99.9999%). It was positioned in a tube furnace, shown in Fig. 1a. Sulfur lumps and precursors were placed in a quartz glass container. The quartz containers were placed in a tubular furnace in  $\text{N}_2$  gas flow (10 sccm) under atmospheric pressure. The furnace was heated to the specified sulfurization temperatures (500, 520, 530, 540, 570, 600  $^{\circ}\text{C}$ ) in a nitrogen atmosphere at 10  $^{\circ}\text{C}/\text{min}$  for 2 h, and then allowed to cool naturally. The temperature sequence is shown in Fig. 1b. The obtained CTS thin films were etched by immersing them in deionized water for 30 min to remove residual NaF and Na compounds.

The samples were analyzed as follows: (1) Evaluation of elemental composition ratio by inductively coupled plasma (ICP) atomic emission spectroscopy (Shimadzu, ICPS-7510), (2) Phase identification by X-ray diffraction (XRD) (Rigaku, Miniflex), (3) Crystal structure identification by Raman spectroscopy (Jasco, RMP-510), (4) Measurement of the photovoltaic characteristics of solar cells with the CTS film as the absorption layer. Based on these results, samples for PL observation were chosen.

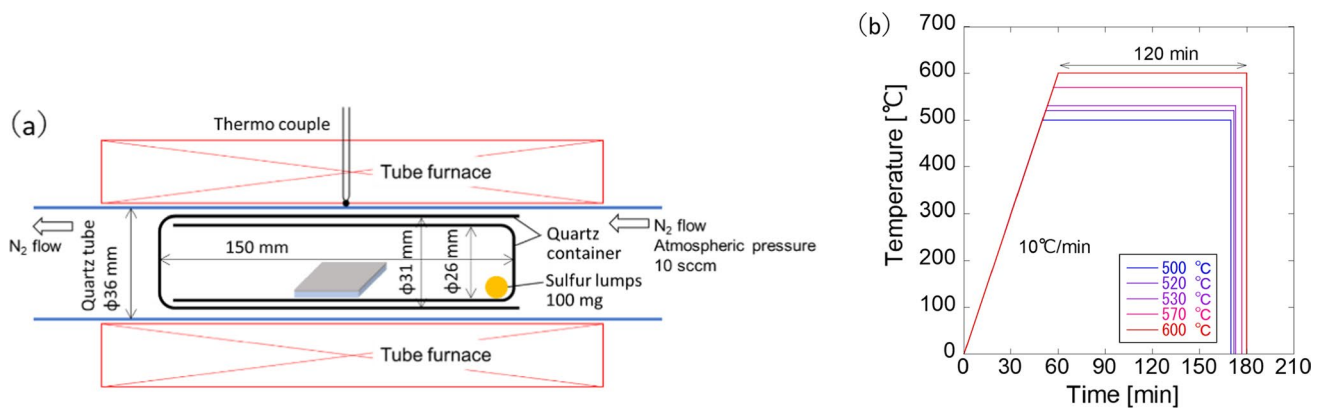
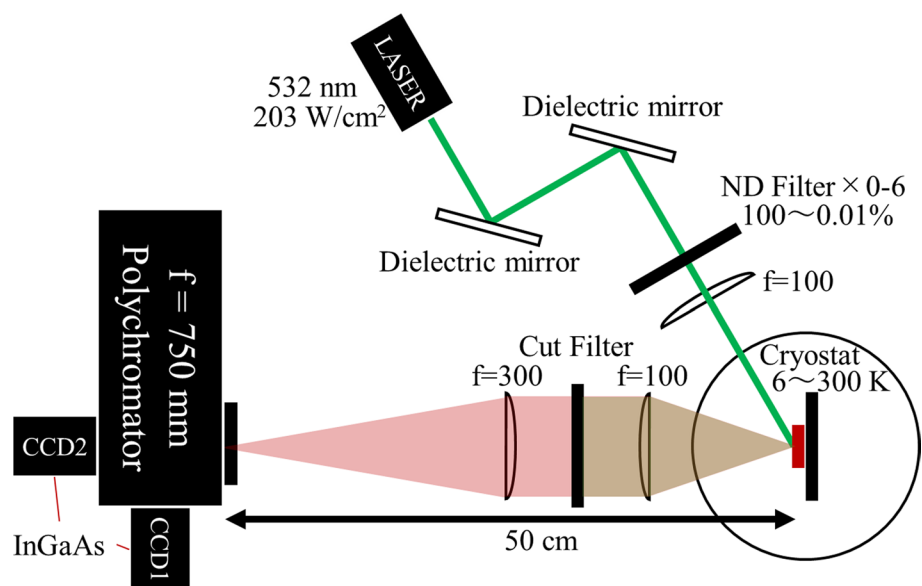


**Fig. 1** **a** Layout of glass container, samples and sulfur sources in a sulfurization tube furnace. **b** Temperature sequence of sulfurization process

**Fig. 2** PL observation system



The PL spectra were observed using the optical system shown in Fig. 2. The excitation was from  $\text{Nd}^{3+}:\text{YVO}_4$  second harmonic laser light of wavelength 532 nm with power density of  $203 \text{ W/cm}^2$ . The PL was dispersed by a 750 mm polychromator (Andor, Shamrock 750) and detected by InGaAs CCDs (Andor, iDus DU490A-1.7 and iDus DU490A-2.2). For the measurement of excitation intensity dependence, the intensity of the excitation light was changed in the range of 100–0.01% of  $203 \text{ W/cm}^2$  by using several neutral density (ND) filters. In the temperature-dependent measurements, the cryostat (Pascal, Pascal-OPS101) temperature was varied in the range of 6–300 K.

### 3 Results and discussion

As shown in Table 1, ICP atomic emission spectroscopy analysis confirmed that all CTS thin films had an ideal Cu-poor ( $\text{Cu}/\text{Sn} < 2.0$ ) composition for high-efficiency

**Table 1** Summary of measurement results.  $M/(M+C)$  is the monoclinic/(monoclinic + cubic) percentage (adapted from Ref. [22])

Sulfurize temperature (°C)	ICP		$M/(M+C)$	Efficiency (%)
	Cu/Sn	Na/(Na+Cu)		
500	1.70	0.081	55.43	0.025
520	1.68	0.090	63.18	0.176
530	1.72	0.083	63.14	0.115
570	1.75	0.065	100	1.665
600	1.78	0.070	100	2.497

CTS solar cells. As shown in Fig. 3a, from the XRD results, peaks were observed that could be attributed to CTS; however, since the diffraction angles of the peaks for monoclinic and cubic CTS are almost the same, the crystal structures could not be distinguished [22].

To identify the crystal structures of the CTS thin films, Raman spectra were measured. The Raman peaks were deconvoluted into 7 peaks at  $222\text{ cm}^{-1}$ ,  $261\text{ cm}^{-1}$ ,  $290\text{ cm}^{-1}$ ,  $303\text{ cm}^{-1}$ ,  $319\text{ cm}^{-1}$ ,  $353\text{ cm}^{-1}$  and  $372\text{ cm}^{-1}$  as shown in Fig. 3b. The peaks at  $290\text{ cm}^{-1}$ ,  $319\text{ cm}^{-1}$ ,  $353\text{ cm}^{-1}$ , and  $372\text{ cm}^{-1}$  are attributed to monoclinic structure [23] and  $303\text{ cm}^{-1}$  is attributed to cubic structure [13]. From the peaks at  $303\text{ cm}^{-1}$  and at  $290\text{ cm}^{-1}$  ratio of the monoclinic phase/(monoclinic phase + cubic phase) ratio at each temperature were calculated. The results are shown in Table 1.

Conversion efficiency of the solar cells with the CTS thin films sulfurized at several temperature was shown in Table 1. The conversion efficiency of the solar cells consisting cubic CTS is lower than that of the solar cells consisting only monoclinic.

Based on the above results, to observe the PL spectra, we decided to choose two samples with poor conversion efficiency, sulfurized at 520 and 530 °C, and two samples with high conversion efficiency, sulfurized at 570 and 600 °C.

Figure 4 shows PL spectra observed at 6 K from the CTS thin films sulfurized at 520 and 530 °C (here after referred to as samples of 520 and 530 °C), which contained cubic CTS and from the CTS sulfurized at 570 and 600 °C (here after referred to as samples of 570 and 600 °C), which contained no cubic CTS. All spectra were normalized to the intensity value at 0.775 eV. For the samples of 520 and 530 °C, weak and broad luminescence was observed in the low-energy band, the values were multiplied by 10 after normalization. As can be seen from Fig. 4, the PL spectra of the samples of 600 °C and 570 °C show peaks at around 0.83, 0.86, and 0.94 eV, and the PL spectra of the samples of 530 °C and

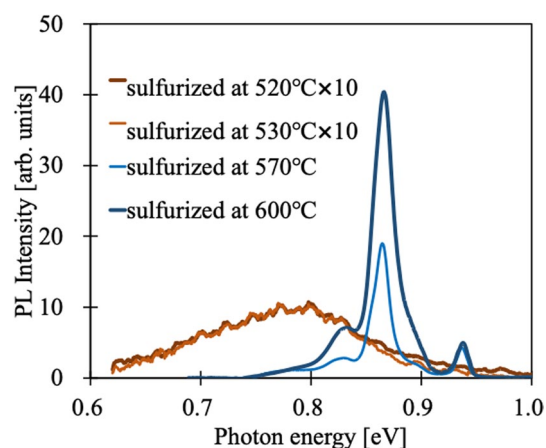


**Fig. 4** Normalized PL spectra of CTS thin films sulfurized at 520, 530, 570 and 600 °C, respectively. The PL spectra were normalized by the intensity at 0.775 eV. For the samples of 520 and 530 °C, the values were multiplied by 10 after normalization

520 °C show around 0.78 eV. The spectrum includes more than aforementioned peaks, and the spectrum needs to be resolved and discussed. However, since the PL spectra of the samples of 520 and 530 °C show the same tendency, and the PL spectra of the samples of 570 and 600 °C are similar, in the following discussion, we will focus on the samples of 520 and 600 °C.

To investigate the origin of the PL, the dependence of the PL spectra on the excitation intensity and observation temperature was observed for the samples of 520 and 600 °C.

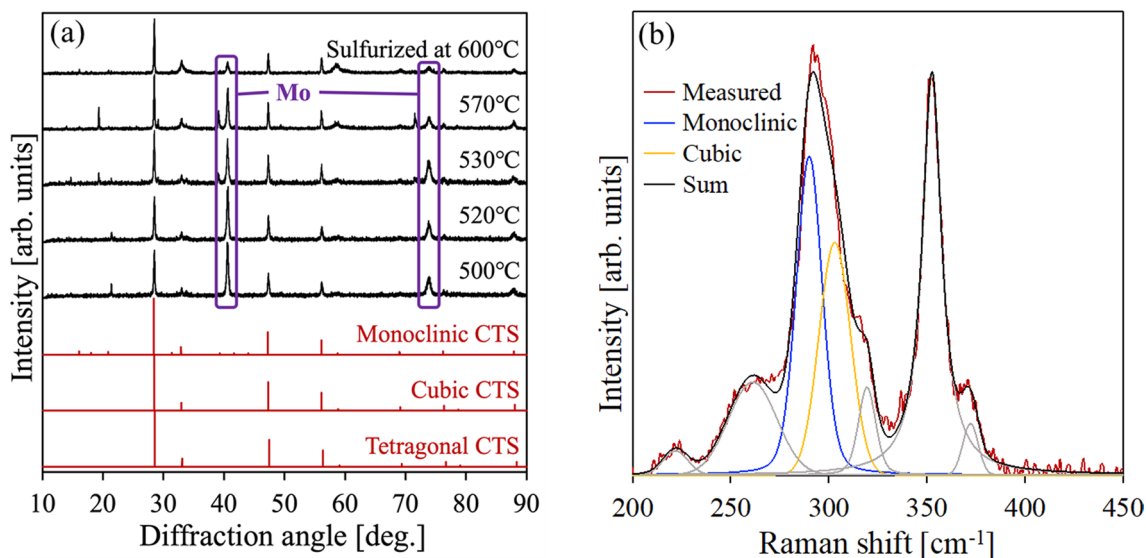


**Fig. 3** **a** XRD results for the CTS thin films sulfurized at different temperatures. **b** Raman scattering spectrum for CTS thin film sulfurized at 500 °C. The spectrum was deconvoluted into peaks due to the monoclinic and cubic structures (adapted from Ref. [22])

The PL spectra at 6 K for the samples of 520 and 600 °C as a function of excitation intensity are shown in Fig. 5a, b, respectively. The spectrum of the sample of 520 °C is wavy, which probably due to Fabry–Perot interference. This broadening of the PL spectrum for the 520 °C sample is similar to that in Ref. [24].

The temperature dependence of PL spectra for the samples of 520 and 600 °C are shown in Fig. 6a, b, respectively. The excitation intensity is 100% for the sample of 520 °C, and 9.1% for the sample of 600 °C. At room temperature, for the sample of 600 °C, a narrow peak around 0.94 eV was observed, while for the sample of 520 °C only very weak and broad luminescence was observed. The PL spectrum of the sample of 600 °C at room temperature is very similar to results shown in ref [10].

As shown in Fig. 6b, PL from the sample of 600 °C has a narrow luminescence peak at around 0.94 eV and broad luminescence at 0.8–0.9 eV. PL from the sample of 520 °C only shows a very broad luminescence peak at 0.6–0.9 eV. From our previous work, the narrow and wide luminescence peaks correspond to exciton luminescence and DAP recombination luminescence, respectively [21].

As shown in Fig. 6b, the spectrum of the sample of 600 °C is composed of several peaks. Therefore, the spectrum was resolved into several Gaussian peaks. Figure 7 shows the resolved PL of the sample of 600 °C with excited 9.1% (18.5  $\text{W}/\text{cm}^2$ ).

As shown in Fig. 7, the spectrum can be fitted with 8 peaks, and the peaks are named p1–p8 from lower to higher

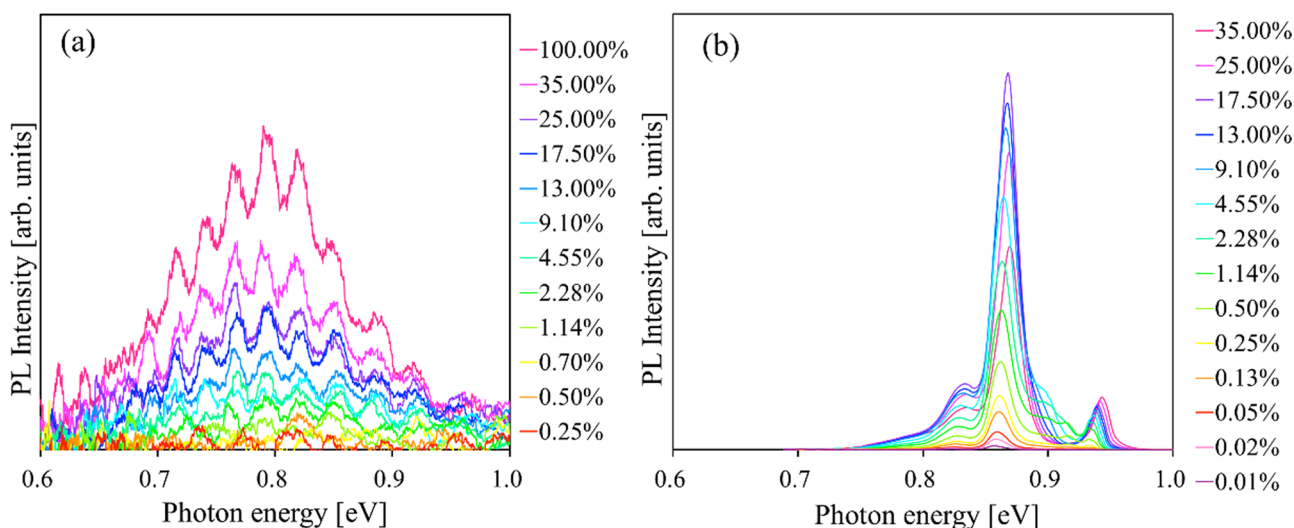


**Fig. 5** Excitation intensity dependence of PL spectrum for CTS thin films sulfurized at **a** 520 °C, sulfurized at **b** 600 °C

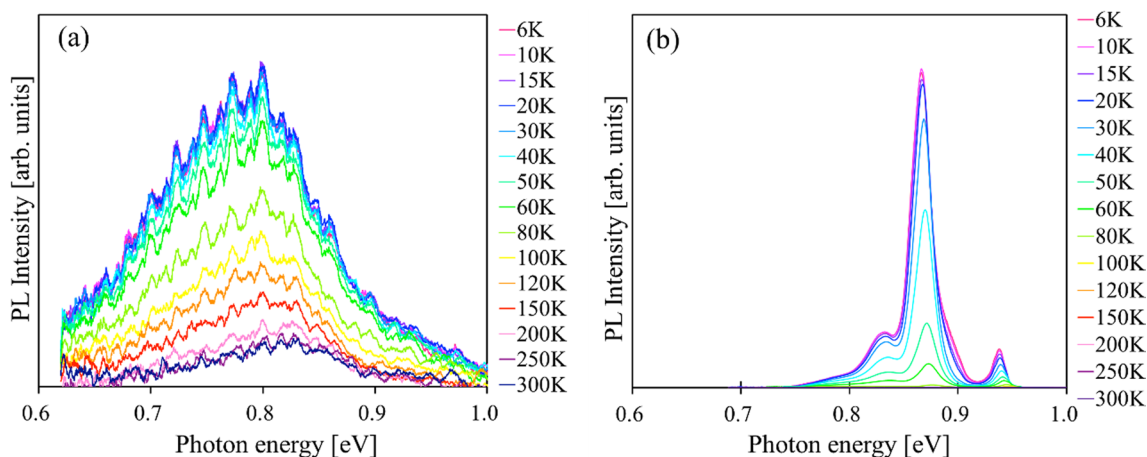


**Fig. 6** Temperature-dependent PL spectrum for CTS thin films sulfurized at **a** 520 °C, sulfurized at **b** 600 °C

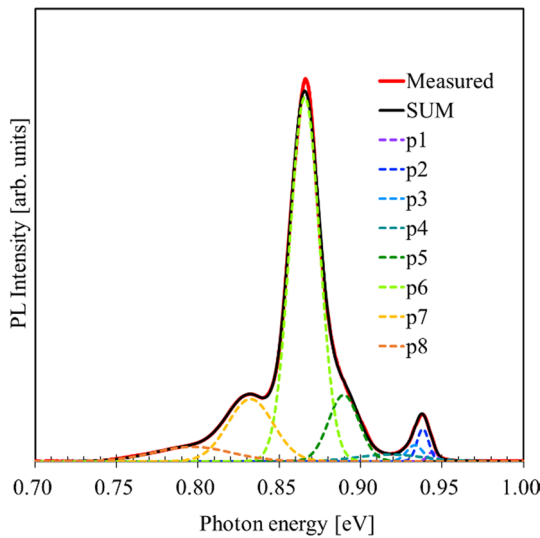


**Fig. 7** Resolved PL spectrum of the CTS thin film sulfurized at 600 °C

**Table 2** Peak energy of the Resolved PL spectrum of the CTS thin film sulfurized at 600 °C (Fig. 7)

Peak name	$E_{Res}$ (meV)
p1	943.9
p2	938.2
p3	933.2
p4	918.1
p5	889.5
p6	865.6
p7	832.3
p8	796.5

energy. The peak energy of the each peak is shown in Table 2.

The spectrum of the sample of 600 °C contains 8 peaks. However, the spectrum of the sample of 520 °C is composed of two peaks, whose peak energies are almost the same as p7 and p8 for the sample of 600 °C. Therefore, it is assumed that the origins of both peaks are as the same as p7 and p8, and they were named p7' and p8'.

The relationship between the excitation light intensity ( $P_{exc}$ ) and the luminescence intensity ( $I_{PL}$ ) is well known as:

$$I_{PL} \propto P_{exc}^\gamma, \tag{1}$$

where  $\gamma$  is a derived parameter, and the luminescence mechanism can be determined from the numerical value of  $\gamma$ ; typically,  $\gamma > 1$  for exciton recombination luminescence, and  $\gamma < 1$  for DAP recombination luminescence or free-to-bound (FB) recombination luminescence [25, 26].

Generally, the peak energy of DAP recombination luminescence shifts to higher energy as the excitation

light intensity increases, and the peak shift rate is less than ~ 10 meV/decade [27]. The light luminescence mechanism was elucidated by integrating the above results for  $\gamma$  and the peak shift rate.

To determine the activation energy associated with these luminescence peaks, the temperature dependence was investigated. The exciton luminescence relationship between the sample temperature  $T$  and the luminescence intensity  $I_{ex}$  is well known as:

$$I_{ex}(T) = \frac{I_0}{1 + C \exp\left(-\frac{E_{ex}}{k_B T}\right)}, \tag{2}$$

where  $I_0$  is the intensity of the luminescence at 0 K,  $C$  is a constant,  $k_B$  is Boltzman's constant, and  $E_{ex}$  is activation energy [28]. For DAP recombination luminescence, the relationship between  $T$  and the luminescence intensity  $I_{DAP}$  is well known as:

$$I_{DAP}(T) = \frac{I_0}{1 + \alpha T^{\frac{3}{2}} + \beta T^{\frac{3}{2}} \exp\left(-\frac{E_a}{k_B T}\right)}, \tag{3}$$

where  $I_0$  is the intensity of the luminescence at 0 K,  $\alpha$  and  $\beta$  are DAP recombination luminescence parameters,  $k_B$  is Boltzman's constant, and  $E_a$  is the activation energy [29].

The activation energy was obtained by fitting the Arrhenius plot from the temperature dependence of luminescence peak areas with the above equations. The donor level or acceptor level on the other side of  $E_b$  is calculated by the following formula.

$$E_b = E_g - E_{PL} - E_a, \tag{4}$$

where  $E_g$  is the estimated band gap energy,  $E_{PL}$  is the peak energy, and  $E_a$  is the activation energy.

Figure 8a, b show the Arrhenius plots of samples of 520 °C and 600 °C, respectively. The activation energy was calculated by fitting the plots with Eqs. (2) or (3).

In Table 3,  $E_{PL}$  is the averaged peak energy for all excitation intensities,  $\gamma$  is a parameter from Eq. (1), p-shift is the peak shift rate from the excitation intensity dependence, luminescence origin is the origin of luminescence obtained from  $\gamma$  and p-shift, and  $E_a$  and  $E_b$  are activation energies from Eqs. (2)–(4).

First, we discuss the sample of 600 °C with high conversion efficiency. From Table 3, since  $\gamma$  of p1–p3 is larger than 1 and the peak energy is near the reported exciton luminescence [21], p1–p3 were attributed to exciton luminescence. In Ref. [30],  $E-k$  curves, which were drawn from the results of first-principles calculations, show that the top of the valence band is split into three levels. This corresponds to p1–p3 of the peaks resolved in this study. Therefore, p1–p3

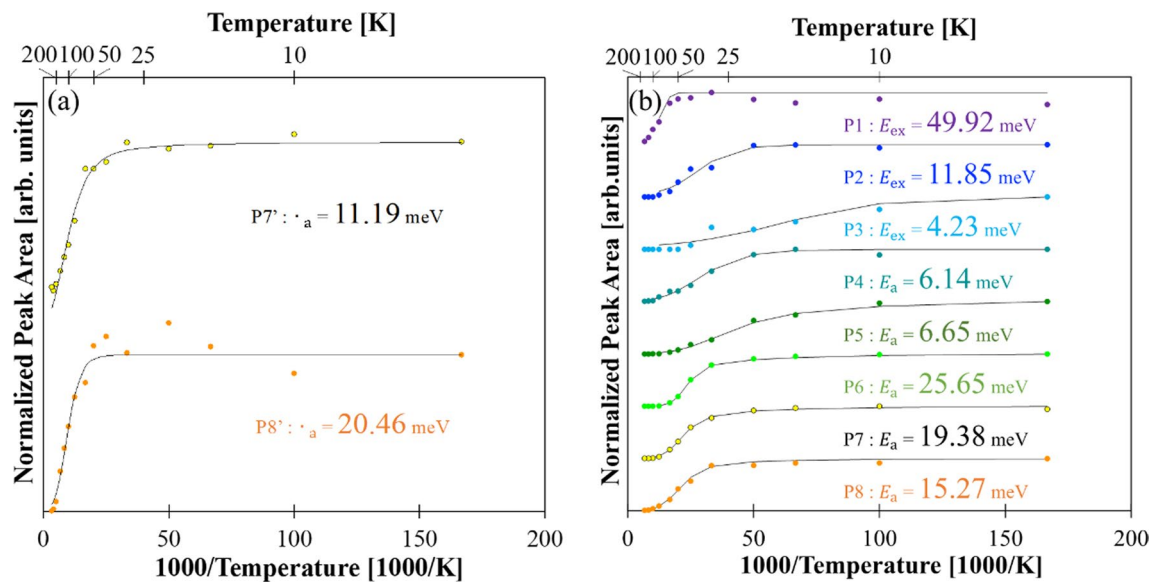


**Fig. 8** Arrhenius plots of peak areas for CTS thin film sulfurized at **a** 520 °C, sulfurized at **b** 600 °C

**Table 3** The excitation intensity dependence and temperature dependence results for the CTS thin films sulfurized at 520 and 600 °C

Peak name	$E_{PL}$ (meV)	$\gamma$	p-shift (meV)	Luminescence origin	$E_{ex}$ or $E_a$ (meV)	$E_b$ (meV)
p1	943.9	1.57	0	Exciton	49.92	–
p2	938.2	1.19	0	Exciton	11.85	–
p3	933.2	1.12	0	Exciton	4.23	–
p4	912.7	1.09	5.59	DAP	6.14	16.9
p5	881.8	0.74	11.95	DAP	6.65	47.7
p6	861.3	0.67	3.11	DAP	25.65	50.4
p7	827.8	0.63	3.51	DAP	19.38	90.4
p7'	(827.8)	–	–	(DAP)	11.19	98.6
p8	794.6	0.61	1.86	DAP	15.27	127.6
p8'	(794.6)	–	–	(DAP)	20.46	122.4

are considered to be derived from exciton luminescence related to the separated valence bands.

As mentioned above, p1–p3 are attributed to exciton luminescence. If the temperature is higher than the temperature corresponding to the exciton binding energy, the excitons dissociate and show band-edge luminescence. Therefore, the exciton binding energy was estimated from the values below 80 K in the Arrhenius plot of Eq. (2).

When the exciton of p3 dissociates and becomes band-edge luminescence, the peak energy shifts to the higher energy side and overlaps the p1 and p2 luminescence. Therefore, at higher temperature, p1 and p2 cannot be separated well due to the overlap with p3, and the apparent activation energy becomes higher. Luminescence is observed at around 0.94 eV even at room temperature. This luminescence is the band-edge luminescence caused by the dissociated exciton and thermal excited carriers from donor and acceptor levels.

For p4,  $\gamma$  is a value higher than 1; however, to attribute this p4 to exciton luminescence, one must consider that the peak energy is small, the peak shift dependence on excitation intensity is not zero, and  $\gamma$  is only slightly larger than 1. Therefore, the fact that the value slightly exceeds 1 is considered to be due to measurement error and it is concluded that the origin of p4 can be attributed to DAP recombination luminescence.

For p5, the peak shift is roughly 10 meV/decade and  $\gamma$  is less than 1; therefore, the origin of the p5 is considered to be DAP recombination luminescence.

As shown in Table 3,  $\gamma$  is less than 1 and peak shift is few meV/decade, so p6–p8 are attributed to DAP recombination luminescence.

The bandgap energy can be estimated from the sum of  $E_{ex}$ , which corresponds to the exciton binding energy, and the energy of exciton emission associated with the highest

valence peak p3. The estimated bandgap energy is 0.937 eV, which is very close to the value reported in ref [20].

The  $E_a$  of p4–p6 and  $E_b$  of p4 are relatively small compared to thermal energy at room temperature, and the  $E_b$  of p5 and p6 are on the same order as the thermal energy at room temperature; therefore, defects related to p4–p6 cannot be factor in reducing conversion efficiency because those are not carrier trap source.

The  $E_a$  of p7 and p8 are relatively small compared to the thermal energy at room temperature; however,  $E_b$  of p7 and p8 are large, therefore the defects related to p7 and p8 are very deep and could be factor in reducing the conversion efficiency.

Next, we discuss the sample of 520 °C with low conversion efficiency. As can be seen from Fig. 6a, it was not possible to derive  $\gamma$  or a peak shift, because the spectra are wavy and a sufficient amount of data to determine the excitation intensity dependence could not be obtained due to low luminescence intensity.

The spectral deconvolution results show that the spectrum is composed of two peaks, and the positions of the peaks are almost the same as p7 and p8 of the sample of 600 °C. The values of the activation energy were also close to those of the sample of 600 °C. Therefore, although  $\gamma$  could not be derived, it was speculated that origin of p7' and p8' was DAP recombination luminescence. In this study, p7' and p8' were considered to correspond to p7 and p8 based on their energies, but further investigation is needed to determine if this consideration is valid or not.

Since the p4–p8 of the sample of 600 °C and p7' and p8' of the sample of 520 °C were determined to be DAP recombination luminescence, the donor and acceptor levels of the samples of 520 °C and 600 °C were drawn as shown in Fig. 9a, b, respectively, using calculated  $E_a$  and  $E_b$ . Here, calculated  $E_a$  was considered as acceptor level because CTS is p-type semiconductor.

Based on the above results, samples 520 °C and 600 °C are compared again. The decrease in luminescence intensity with increasing temperature in the sample of 520 °C is slower than in the sample of 600 °C as shown in Fig. 6a, b. As mentioned previously, band-edge luminescence was observed at room temperature for the sample of 600 °C. This is due to thermally dissociated excitons and carriers thermally excited from the donor and acceptor levels. In other words, carriers thermally excited from the donor and acceptor levels are not captured by the donor and acceptor again and are not used for DAP recombination luminescence, resulting in band-edge luminescence. On the other hand, no band-edge luminescence is observed in the sample of 520 °C. Therefore, it is possible that some of the thermally excited carriers are trapped again in the donor and acceptor levels, resulting in DAP recombination luminescence, and the sample of 520 °C would shows a slower decrease

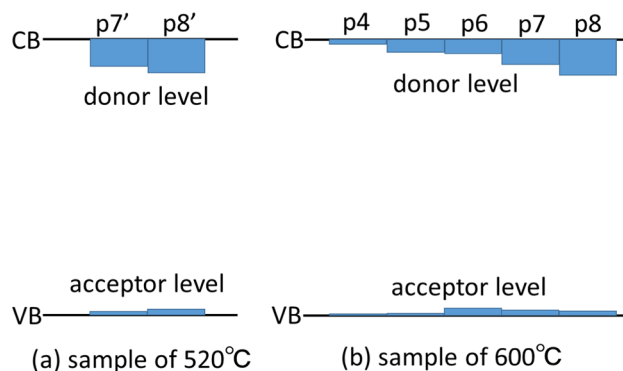


**Fig. 9** Donor and acceptor levels of **a** sample of 520 °C and **b** sample of 600 °C drawn by using calculated  $E_a$  as acceptor levels and  $E_b$  as donor levels. In this figure CB and VB are conduction band and valence band, respectively

in luminescence intensity with increasing temperature than the sample of 600 °C.

The sample of 520 °C contains cubic CTS as well as monoclinic CTS. The band gap of cubic CTS is reported as 0.96 eV [13], which is comparable to that of monoclinic CTS. Therefore, the PL of cubic CTS is expected to be observed in the same energy region as that of monoclinic CTS. There are no reports on PL from cubic CTS, therefore, it is unclear whether the origin of the p7' and p8' observed from the sample of 520 °C is cubic CTS or monoclinic CTS. However, since the luminescence intensity becomes very weak when cubic CTS is included, and since the luminescence energy and activation energy of p7' and p8' are comparable to those of p7 and p8 observed from the sample of 600 °C which containing only monoclinic CTS, it is reasonable to consider that the luminescence from the sample of 520 °C also due to monoclinic CTS. In this case, cubic CTS shows no luminescence. If the cubic CTS has many very deep defects, the carriers trapped there will not contribute to luminescence, so PL will not be observed. Also, the carriers trapped very deep defects would not contribute to electric generation. This corresponds to the very low conversion efficiency of cubic CTS. To confirm these facts, it is necessary to fabricate a sample of cubic alone and investigate whether or not it does not show luminescence.

The efficiency of solar cells is affected not only by recombination in the absorption layer (bulk recombination), but also by recombination in the depletion layer and absorption layer/buffer layer interface recombination. For example, passivation of the CTS surface suppresses interfacial recombination and improves efficiency [31]. Therefore, it is beneficial to study the luminescence of the solar cell if one wants to gain insight into improving the efficiency. The luminescence in this experiment corresponds to the luminescence due to bulk recombination in the solar cell, and recombination in the depletion layer



or interfacial recombination cannot be observed. However, since the fabrication of a solar cell requires many steps, it is useful to be able to roughly determine the efficiency before the device is fabricated, i.e., at the absorption layer preparation stage.

In this investigation, it was found that the CTS thin film of sufficient quality to be utilized in a high-efficiency solar cell showed band-edge luminescence at room temperature, while the CTS thin film which gave a lower efficiency solar cell showed only weak and broad band luminescence. Therefore, it is possible to determine whether a solar cell constructed with a fabricated thin film can be highly efficient or not by simply observing the PL of the CTS thin film at room temperature.

## 4 Conclusions

In this study, PL spectra of the thin films consisting of only monoclinic CTS, sulfurized at higher temperature of 570 and 600 °C, and the thin films consisting with cubic and monoclinic CTS sulfurized at lower temperature of 520 and 530 °C were investigated. Since the PL from CTS thin films sulfurized at the lower two temperatures showed the same tendencies and those sulfurized at the higher temperatures also showed behavior similar to each other, CTS thin films sulfurized at 520 and 600 °C were chosen for further detailed analysis. The analysis showed that the PL spectrum of the CTS thin film sulfurized at 600 °C consisted of 8 peaks. Of these, 3 were associated with exciton luminescence or band-edge luminescence, 3 were due to DAP recombination luminescence with shallow defects as non-carrier trap source, and 2 were due to DAP recombination luminescence from deep defects as the carrier trap source.

The PL spectrum of the CTS thin film sulfurized at 520 °C consisted of 2 peaks, both of which were due to DAP recombination luminescence from deep defects as the carrier trap source. The PL spectra of CTS thin films differed greatly depending on whether cubic structure contained or not. In addition, band-edge luminescence was able to be observed even at room temperature for the thin film consisting only monoclinic CTS, which shows higher conversion efficiency. From the above results, it was shown that the conversion efficiency and crystal structure of CTS thin films can be easily estimated based on PL measurements at room temperature.

**Acknowledgements** This work was supported by JSPS KAKENHI [JP19H02663] and [JP20H02680]. Mr. K. Watanabe supported the sulfurization process of the samples.

**Data availability** The numerical data used to plot the graph are available from the corresponding author on reasonable request.

## References

1. T.A. Kuku, O.A. Fakolujo, Photovoltaic characteristics of thin films of  $\text{Cu}_2\text{SnS}_3$ . *Sol. Energy Mater.* **16**, 199–204 (1987). [https://doi.org/10.1016/0165-1633\(87\)90019-0](https://doi.org/10.1016/0165-1633(87)90019-0)
2. J. Chantana, K. Suzuki, T. Minemoto, Introduction of Na into  $\text{Cu}_2\text{SnS}_3$  thin film for improvement of its photovoltaic performances. *Sol. Energy Mater. Sol. Cells* **168**, 207–213 (2017). <https://doi.org/10.1016/j.solmat.2017.04.040>
3. J. Chantana, K. Tai, H. Hayashi, T. Nishimura, Y. Kawano, T. Minemoto, Investigation of carrier recombination of Na-doped  $\text{Cu}_2\text{SnS}_3$  solar cell for its improved conversion efficiency of 5.1%. *Sol. Energy Mater. Sol. Cells* **206**, 110261 (2020). <https://doi.org/10.1016/j.solmat.2019.110261>
4. A. Kanai, K. Toyonaga, K. Chino, H. Katagiri, H. Araki, Fabrication of  $\text{Cu}_2\text{SnS}_3$  thin-film solar cells with power conversion efficiency of over 4%. *Jpn. J. Appl. Phys.* **54**, 08KC06 (2015). <https://doi.org/10.7567/JJAP.54.08KC06>
5. M. Nakashima, J. Fujimoto, T. Yamaguchi, M. Izaki,  $\text{Cu}_2\text{SnS}_3$  thin-film solar cells fabricated by sulfurization from NaF/Cu/Sn stacked precursor. *Appl. Phys. Exp.* **8**, 042303 (2015). <https://doi.org/10.7567/APEX.8.042303>
6. K. Suzuki, J. Chantana, T. Minemoto, Na role during sulfurization of NaF/Cu/SnS<sub>2</sub> stacked precursor for formation of  $\text{Cu}_2\text{SnS}_3$  thin film as absorber of solar cell. *Appl. Surf. Sci.* **414**, 140–146 (2017). <https://doi.org/10.1016/j.apsusc.2017.04.099>
7. A. Kanai, M. Sugiyama, Na induction effects for J-V properties of  $\text{Cu}_2\text{SnS}_3$  (CTS) solar cells and fabrication of a CTS solar cell over-5.2% efficiency. *Sol. Energy Mater. Sol. Cells* **231**, 111315 (2021). <https://doi.org/10.1016/j.solmat.2021.111315>
8. W. Shockley, H.J. Queisser, Detailed balance limit of efficiency of p-n junction solar cells. *J. Appl. Phys.* **32**, 510 (1961). <https://doi.org/10.1063/1.1736034>
9. M. Onoda, X.A. Chen, A. Sato, H. Wada, Crystal structure and twinning of monoclinic  $\text{Cu}_2\text{SnS}_3$ . *Mater. Res. Bull.* **35**, 1563 (2000). [https://doi.org/10.1016/S0025-5408\(00\)00347-0](https://doi.org/10.1016/S0025-5408(00)00347-0)
10. D.M. Berg, R. Djemour, L. Gütay, G. Zoppi, S. Siebentritt, P.J. Dale, Thin film solar cells based on the ternary compound  $\text{Cu}_2\text{SnS}_3$ . *Thin Solid Films* **520**, 6291–6294 (2012). <https://doi.org/10.1016/j.tsf.2012.05.085>
11. H. Guan, H. Shen, C. Gao, X. He, Structural and optical properties of  $\text{Cu}_2\text{SnS}_3$  and  $\text{Cu}_3\text{SnS}_4$  thin films by successive ionic layer adsorption and reaction. *J. Mater. Sci. Mater. Electron.* **24**, 1490 (2013). <https://doi.org/10.1007/s10854-012-0960-x>
12. H. Zhang, M. Xie, S. Zhang, Y. Xiang, Fabrication of highly crystallized  $\text{Cu}_2\text{SnS}_3$  thin films through sulfurization of Sn-rich metallic precursors. *J. Alloys Compd.* **602**, 199–203 (2014). <https://doi.org/10.1016/j.jallcom.2014.03.014>
13. P.A. Fernandes, P.M.P. Salomé, A.F.D. Cunha, A study of ternary  $\text{Cu}_2\text{SnS}_3$  and  $\text{Cu}_3\text{SnS}_4$  thin films prepared by sulfurizing stacked metal precursors. *J. Phys. D Appl. Phys.* **43**, 215403 (2010). <https://doi.org/10.1088/0022-3727/43/21/215403>
14. R. Chierchia, F. Pigna, M. Valentini, C. Malerba, E. Salza, P. Mangiapane, T. Polichetti, A. Mittig,  $\text{Cu}_2\text{SnS}_3$  based solar cell with 3% efficiency. *Phys. Stat. Sol. C* **13**, 35–39 (2016). <https://doi.org/10.1002/pssc.201510115>
15. S. Sato, H. Sumi, G. Shi, M. Sugiyama, Investigation of the sulfurization process of  $\text{Cu}_2\text{SnS}_3$  thin films and estimation of band offsets of  $\text{Cu}_2\text{SnS}_3$ -related solar cell structure. *Phys. Stat. Sol. C* **12**, 757–760 (2015). <https://doi.org/10.1002/pssc.20140294>
16. N. Aihara, H. Araki, A. Takeuchi, K. Jimbo, H. Katagiri, Fabrication of  $\text{Cu}_2\text{SnS}_3$  thin films by sulfurization of evaporated

- Cu-Sn precursors for solar cells. *Phys. Stat. Sol. C* **10**, 1086–1092 (2013). <https://doi.org/10.1002/pssc.201200866>
17. J. Koike, K. Chino, N. Aihara, H. Araki, R. Nakamura, K. Jimbo, H. Katagiri,  $\text{Cu}_2\text{SnS}_3$  thin-film solar cells from electroplated precursors. *Jpn. J. Appl. Phys.* **51**, 10NC34 (2012). <https://doi.org/10.1143/JJAP.51.10NC34>
  18. N. Aihara, K. Tanaka, H. Uchiki, A. Kanai, H. Araki, Donor-acceptor pair recombination luminescence from monoclinic  $\text{Cu}_2\text{SnS}_3$  thin film. *Appl. Phys. Lett.* **107**, 032101 (2015). <https://doi.org/10.1063/1.4927203>
  19. Y. Matsumoto, N. Aihara, A. Munemura, K. Tanaka, Preparation of monoclinic  $\text{Cu}_2\text{SnS}_3$  single crystal by chemical vapor transport with iodine. *Mater. Lett.* **170**, 213–216 (2016). <https://doi.org/10.1016/j.matlet.2016.02.039>
  20. N. Aihara, Y. Matsumoto, K. Tanaka, Exciton luminescence from  $\text{Cu}_2\text{SnS}_3$  bulk crystals. *Appl. Phys. Lett.* **108**, 092107 (2016). <https://doi.org/10.1063/1.4943229>
  21. K. Tanaka, T. Maeda, H. Araki, Photoluminescence observation of the effects of Cu/Sn ratio and Na addition on  $\text{Cu}_2\text{SnS}_3$ . *Sol. Energy* **199**, 143–151 (2020). <https://doi.org/10.1016/j.solener.2020.02.014>
  22. D. Motai, M. Kobayashi, R. Ohashi, K. Watanabe, Y. Hosokawa, K. Jimbo, Y. Akaki, H. Araki, Sulfurization temperature dependence of Na-added  $\text{Cu}_2\text{SnS}_3$  thin films prepared on an alkali-free substrate. *J. Ternary Multinary Compd.* (2020). [https://doi.org/10.57386/tmc.2020.0\\_44](https://doi.org/10.57386/tmc.2020.0_44)
  23. D.M. Berg, R. Djemour, L. Gütay, S. Siebentritt, P.J. Dale, X. Fontane, V. Izquierdo-Roca, A. Pérez-Rodríguez, Raman analysis of monoclinic  $\text{Cu}_2\text{SnS}_3$  thin films. *Appl. Phys. Lett.* **100**, 192103 (2012). <https://doi.org/10.1063/1.4712623>
  24. Y. Dong, X. Lu, P. Shen, Y. Chen, F. Yue, P. Xiang, L. Sun, P. Yang, J. Chu, Strategic improvement of  $\text{Cu}_2\text{SnS}_3$  thin film by different heating rates and photoluminescence investigation. *Mater. Sci. Semicond. Proc.* **84**, 124–130 (2018). <https://doi.org/10.1016/j.mssp.2018.05.012>
  25. T. Schmidt, K. Lischka, W. Zulehner, Excitation-power dependence of the near-band-edge photoluminescence of semiconductors. *Phys. Rev. B* **45**, 8989–8994 (1992). <https://doi.org/10.1103/PhysRevB.45.8989>
  26. J.P. Teixeira, R.A. Sousa, M.G. Sousa, A.F. da Cunha, P.A. Fernandes, P.M.P. Salome, J.C. Gonzalez, J.P. Leitao, Comparison of fluctuating potentials and donor-acceptor pair transitions in a Cu-poor  $\text{Cu}_2\text{ZnSnS}_4$  based solar cell. *Appl. Phys. Lett.* **105**, 63901 (2014). <https://doi.org/10.1063/1.4899057>
  27. I. Dirnstorfer, M. Wagner, D.M. Hofmann, M.D. Lampert, F. Karg, B.K. Meyer, Characterization of  $\text{CuIn(Ga)Se}_2$  thin films. *Phys. Stat. Sol. A* **168**, 163–175 (1998). [https://doi.org/10.1002/\(SICI\)1521-396X\(199807\)168:1%3C163::AID-PSSA163%3E3.0.CO;2-T](https://doi.org/10.1002/(SICI)1521-396X(199807)168:1%3C163::AID-PSSA163%3E3.0.CO;2-T)
  28. K. Tanaka, R. Mori, Photoluminescence properties and defects in  $\text{CuBr}_{1-x}\text{I}_x$  thin films and their dependence on halogen ratio. *J. Sol. State. Chem.* **293**, 121786 (2021). <https://doi.org/10.1016/j.jssc.2020.121786>
  29. N. Aihara, Y. Matsumoto, K. Tanaka, Photoluminescence characterization of  $\text{Cu}_2\text{GeS}_3$  bulk crystals. *Phys. Stat. Sol. B* **254**, 1700118 (2017). <https://doi.org/10.1002/pssb.201700118>
  30. A. Crovetto, R. Chen, R.B. Ettliger, A.C. Cazzaniga, J. Schou, C. Persson, O. Hansen, Dielectric function and double absorption onset of monoclinic  $\text{Cu}_2\text{SnS}_3$ : origin of experimental features explained by first-principles calculations. *Sol. Energy Mater. Sol. Cells* **154**, 121–129 (2016). <https://doi.org/10.1016/j.solmat.2016.04.028>
  31. A. Kanai, M. Sugiyama, Emission properties of intrinsic and extrinsic defects in  $\text{Cu}_2\text{SnS}_3$  thin films and solar cells. *Jpn. J. Appl. Phys.* **60**, 015504 (2021). <https://doi.org/10.35848/1347-4065/abcf06>

**Publisher's Note** Springer Nature remains neutral with regard to jurisdictional claims in published maps and institutional affiliations.

Springer Nature or its licensor (e.g. a society or other partner) holds exclusive rights to this article under a publishing agreement with the author(s) or other rightsholder(s); author self-archiving of the accepted manuscript version of this article is solely governed by the terms of such publishing agreement and applicable law.